Accurate estimate of turbulent dissipation rate using PIV data

Duo Xu, Jun Chen *

School of Mechanical Engineering, Purdue University, West Lafayette, IN 47907, USA

ARTICLE INFO

ABSTRACT

Quantifying the turbulent dissipation rate provides insight into the physics of the turbulent flows. However, the accuracy of estimating turbulent dissipation rate using velocity data measured by planar PIV is affected by the way of modeling the unresolved velocity gradient terms and the PIV spatial resolution. In this paper, we first give a brief review of different methods used to estimate turbulent dissipation rate. Then synthetic PIV data are generated from a turbulence DNS dataset for validating the effectiveness of different methods. Direct estimate of turbulent dissipation rate from its definition using velocity gradients, with the assumption of isotropy, local axisymmetry, or local isotropy, shows significant decrease as interrogation window size increases. On the other hand, the indirect estimation of turbulent dissipation rate from energy spectra and structure function demonstrate less severe decrease as interrogation window size increases. We further propose two modified methods. The *Modified Structure Function Method* relies on an empirical relationship established by analyzing the synthetic PIV data. For a given measured value turbulent dissipation rate under a given interrogation window size, the true value can be determined from this relationship. The *Modified Spectra Curvefit Method* accounts the averaging effect introduced by the interrogation window in PIV processing algorithm and thus gives a better calculation of the energy spectra. When the new spectra data are used to curve fit the $-5/3$ slope, an improved estimate of turbulent dissipation rate is expected. Both modified methods are applied to experimental PIV data acquired from a turbulent jet experiment. They give nearly converged estimates of turbulent dissipation rate and Kolmogorov scale at different interrogation window sizes.

© 2012 Elsevier Inc. All rights reserved.

1. Introduction

In turbulence research it is important to understand the physics of turbulent flows, particularly, energy transfer from large-scale mean flow to small-scale turbulence and the viscous energy dissipation, by examining the energy budget. According to Kolmogorov's similarity hypothesis, the turbulence statistics in a small-scale universal equilibrium range is uniquely determined by the kinematic viscosity of the fluid v and turbulent dissipation rate ϵ[1] [13,28,20], in which

$$\epsilon \equiv 2v\langle s_{ij}s_{ij}\rangle, \tag{1}$$

where $\langle\cdot\rangle$ represents an averaging operation. s_{ij} is the fluctuating rate of strain expressed using velocity fluctuations $\mathbf{u}' \equiv \mathbf{u} - \langle\mathbf{u}\rangle$ [20], i.e.,

$$s_{ij} \equiv \frac{1}{2}\left(\frac{\partial u_i'}{\partial x_j} + \frac{\partial u_j'}{\partial x_i}\right). \tag{2}$$

Among these two parameters, v is a property of the fluid and ϵ is thus the only flow variable that characterizes the state of turbulence. The significance of ϵ has been extensively addressed in numerous literatures (e.g., [17,3,22,5]). In order to analyze ϵ directly from Eq. (1), all nine elements of fluctuating velocity gradient tensor,

$$\frac{\partial u_i'}{\partial x_j} = \begin{bmatrix} \dfrac{\partial u_1'}{\partial x_1} & \dfrac{\partial u_1'}{\partial x_2} & \dfrac{\partial u_1'}{\partial x_3} \\ \dfrac{\partial u_2'}{\partial x_1} & \dfrac{\partial u_2'}{\partial x_2} & \dfrac{\partial u_2'}{\partial x_3} \\ \dfrac{\partial u_3'}{\partial x_1} & \dfrac{\partial u_3'}{\partial x_2} & \dfrac{\partial u_3'}{\partial x_3} \end{bmatrix}, \tag{3}$$

must be available.

Particle Image Velocimetry (PIV) has been widely used in measuring turbulent flows and analyzing turbulent characteristics including turbulent dissipation rate. The technical details of PIV can be found in, e.g., Raffe et al. [21] and Adrian and Westerweel [1]. Due to the planar (2D) nature of this technique, only 4 out of 9 velocity gradient elements in Eq. (3) can be directly measured, i.e., $\partial u_1'/\partial x_1$, $\partial u_1'/\partial x_2$, $\partial u_2'/\partial x_1$, and $\partial u_2'/\partial x_2$ if the measurements are in x_1-x_2 plane. When the flow is incompressible, $\partial u_3'/\partial x_3$ can be obtained by applying divergence free continuity equation

---

* Corresponding author. Tel.: +1 765 494 7050; fax: +1 765 494 0530.
  E-mail address: junchen@purdue.edu (J. Chen).
[1] The complete name of ϵ is *dissipation rate of turbulent kinetic energy*. In this paper *turbulent dissipation rate* is used for short.

Nomenclature

$\partial u'_i/\partial x_j$	fluctuating velocity gradient tensor
v	kinematic viscosity of the fluid
ϵ_m	measured value of the turbulent dissipation rate
ϵ	turbulent dissipation rate
$\langle \cdot \rangle$	averaging operator
s_{ij}	fluctuating rate of strain
$\mathbf{u}$	flow velocity, $\mathbf{u} \equiv (u, v, w) \equiv (u_1, u_2, u_3)$
$\mathbf{u}'$	fluctuating velocity, $\mathbf{u}' \equiv \mathbf{u} - \langle \mathbf{u} \rangle$
$\mathbf{k}$	wavenumber vector, $\mathbf{k} = (k_1, k_2, k_3)$
$E_{ij}k_1$	one dimensional energy spectrum
$R_{ij}(\mathbf{r}, t)$	two-point velocity correlation
$\mathbf{x}$	location vector
$\mathbf{r}$	displacement vector
$E_{ii}(k_i)$	longitudinal energy spectrum
C_k	Kolmogorov constant
$D_{ij}(\mathbf{r}, t)$	the second-order velocity structure function
$D_{LL}(r)$	longitudinal structure function
Δ	interrogation window size
η	Kolmogorov length scale
δ	spatial resolution of DNS dataset
δ_t	temporal resolution of DNS dataset
E_t	total turbulent kinetic energy
k	magnitude of wavenumber vector, $k = |\mathbf{k}|$
u_{rms}	rms velocity fluctuation
λ	Taylor micro scale

Re_λ	Taylor-scale Reynolds number
τ_η	Kolmogorov time scale
L	turbulent integral length scale
T_L	large eddy turnover time
$\bar{\mathbf{u}}^\Delta$	synthetic PIV velocity with filter window size Δ in *Filtered-PIV-Dataset*
G_Δ	filtering kernel
$\otimes$	convolution operator
H	Heaviside function
$D_{LL}^m(r)$	measured value of $D_{LL}(r)$
σ	standard deviation
α_i	coefficients of curve-fit function
β_i	coefficients of curve-fit function
$\tilde{E}_{11}(k_1)$	longitudinal energy spectrum computed using PIV data
$\tilde{G}(k_1)$	Fourier transform of the filter kernel G
U	initial injection velocity
D	inside diameter of jet nozzle
$\epsilon_{g,m}$	turbulent dissipation rate estimated by velocity gradients method
β_Δ	correction coefficient
ϵ_g	turbulent dissipation rate estimated from gradient methods after β_Δ correction
η_m	measured value of Kolmogorov length scale
$\tilde{\mathbf{u}}^\Delta$	synthetic PIV velocity with interrogation window size Δ in *Synthetic-PIV-Dataset*

$$\frac{\partial u'_3}{\partial x_3} = -\left(\frac{\partial u'_1}{\partial x_1} + \frac{\partial u'_2}{\partial x_2}\right). \tag{4}$$

The other four gradient elements ($\partial u'_1/\partial x_3, \partial u'_2/\partial x_3, \partial u'_3/\partial x_1$, and $\partial u'_3/\partial x_2$), however, cannot be measured by PIV and must be appropriately modeled in order to compute ϵ from Eq. (1).

Despite of the existing efforts (as summarized in Section 2), analyzing turbulent dissipation rate using PIV data is still a challenging task. Different assumptions on unresolved velocity gradient terms and the PIV resolution introduce significant differences to the estimated values of ϵ. Particularly, some of the correction methods rely on prior knowledge of turbulence statistics like Kolmogorov scale. In addition, although the discrepancy between measured and the true values of ϵ can be described qualitatively, quantitative description at different PIV resolutions need to be explored more elaborately.

In this paper, we develop correction methods for estimating ϵ by examining synthetic PIV velocity data generated using a Direct Numerical Simulation (DNS) dataset. The methods are then applied to experimentally acquired PIV data to further demonstrate their effectiveness. The paper is organized as follows. Different methods of estimating ϵ are reviewed in Section 2. Generation of synthetic PIV data is discussed in Section 3. Applications of different methods on synthetic PIV data are given in Section 4. Section 5 presents details of the new method. Results of applying different methods on experimental PIV data are given in Section 6. The final section gives a summary and outlook.

2. Analysis of ϵ using PIV data – a review

2.1. Assumption of isotropy

If one assumes that the turbulent flow is homogeneous and isotropic, ϵ can be analyzed using velocity gradient measured along one direction [19,10,8], i.e.,

$$\epsilon = 15v\left\langle \left(\frac{\partial u'_1}{\partial x_1}\right)^2 \right\rangle. \tag{5}$$

This method is easy to implement, but it does not utilize all the resolved components of fluctuating velocity gradient tensor other than $\partial u'_1/\partial x_1$ in PIV measurements.

2.2. Assumption of local axisymmetry

George and Hussein [8] propose that small scale turbulence can be better described as locally axisymmetric. Once the axisymmetric axis is identified (taken as x_1 in this paper, for example), this assumption leads to an estimate of dissipation rate using the four resolved velocity gradients in PIV

$$\epsilon = v\left\langle -\left(\frac{\partial u'_1}{\partial x_1}\right)^2 + 8\left(\frac{\partial u'_2}{\partial x_2}\right)^2 + 2\left(\frac{\partial u'_1}{\partial x_2}\right)^2 + 2\left(\frac{\partial u'_2}{\partial x_1}\right)^2 \right\rangle. \tag{6}$$

Eq. (6) is also derived for outside the wall region of duct flow by Antonia et al. [2]. To apply this method, the axisymmetric axis must be pre-determined, and different selections result in differences in ϵ.

2.3. Assumption of local isotropy

Doron et al. [7] estimate ϵ in the ocean bottom boundary layer using all the available velocity components from PIV measurements. The unresolved velocity gradient terms in Eq. (1) are expressed by a less constraining local isotropy assumption, i.e.,

$$\left\langle \left(\frac{\partial u'_1}{\partial x_3}\right)^2 \right\rangle = \left\langle \left(\frac{\partial u'_3}{\partial x_1}\right)^2 \right\rangle = \left\langle \left(\frac{\partial u'_2}{\partial x_3}\right)^2 \right\rangle = \left\langle \left(\frac{\partial u'_3}{\partial x_2}\right)^2 \right\rangle$$
$$= \frac{1}{2}\left\langle \left(\frac{\partial u'_1}{\partial x_2}\right)^2 + \left(\frac{\partial u'_2}{\partial x_1}\right)^2 \right\rangle, \tag{7}$$

$$\left\langle \frac{\partial u_1'}{\partial x_3}\frac{\partial u_3'}{\partial x_1}\right\rangle = \left\langle \frac{\partial u_2'}{\partial x_3}\frac{\partial u_3'}{\partial x_2}\right\rangle = \left\langle \frac{\partial u_1'}{\partial x_2}\frac{\partial u_2'}{\partial x_1}\right\rangle. \tag{8}$$

Substituting Eqs. (4), (7) and (8) into Eq. (1), one obtains an expression of ϵ using measured velocity components in x_1-x_2 plane:

$$\epsilon = v\left\langle 4\left(\frac{\partial u_1'}{\partial x_1}\right)^2 + 4\left(\frac{\partial u_2'}{\partial x_2}\right)^2 + 3\left(\frac{\partial u_1'}{\partial x_2}\right)^2 + 3\left(\frac{\partial u_2'}{\partial x_1}\right)^2 \right.$$
$$\left. + 4\left(\frac{\partial u_1'}{\partial x_1}\frac{\partial u_2'}{\partial x_2}\right) + 6\left(\frac{\partial u_1'}{\partial x_2}\frac{\partial u_2'}{\partial x_1}\right)\right\rangle. \tag{9}$$

The dissipation rate estimated using this method has also been applied to study structures in the upper layer of the ocean (e.g., [26]).

2.4. Estimate of ϵ from energy spectra

Another approach of estimating ϵ is to examine one-dimensional energy spectra

$$E_{ij}(k_1) = \frac{1}{\pi}\int_{-\infty}^{\infty} R_{ij}(\mathbf{r})e^{-ik_1 r_1}dr_1, \tag{10}$$

where $\mathbf{k} = \{k_1, k_2, k_3\}$ is wavenumber vector (e.g., [20]). R_{ij} is the two-point correlation

$$R_{ij}(\mathbf{r},t) = \left\langle u_i'(\mathbf{x},t)u_j'(\mathbf{x}+\mathbf{r},t)\right\rangle. \tag{11}$$

ϵ can then be obtained by integrating the one-dimensional dissipation spectrum [19], e.g.,

$$\epsilon = \frac{15}{2}v\left\langle\left(\frac{\partial u_j'}{\partial x_i}\right)^2\right\rangle = \frac{15}{2}v\left\langle\int_0^{\infty} k_i^2 E_{jj}(k_i)dk_i\right\rangle, \tag{12}$$

when local isotropy is assumed (no summation over repeated indices "*i*" and "*j*" here). We denote this method as *spectra integral method*. Ståhl Wernersson and Trägårdh [25] apply this method to study the turbulent flow inside a turbine-agitated tank.

An alternative approach is to estimate ϵ from the curve of $E_{ii}(k_j)$. According to Kolmogorov's energy cascade theory (see, e.g., [28,11,20]), in the inertial subrange, we have

$$E_{ii}(k_i) = \frac{18}{55}C_k\epsilon^{2/3}k_i^{-5/3}, \tag{13}$$

where C_k is the Kolmogorov constant. If one can identify the inertial subrange of $E_{ii}(k_i)$ and apply a $k_i^{-5/3}$ curve fit, one of the curve coefficients is $18/55C_k\epsilon^{2/3}$. ϵ can then be computed

$$\epsilon = \left(\frac{55}{18C_k}k_i^{5/3}\cdot E_{ii}(k_i)\right)^{3/2}. \tag{14}$$

This method is denoted as *spectra curvefit method* in this paper. Doron et al. [7] apply this method to study the turbulence characteristics in the coast ocean bottom boundary layer measured by a submersible PIV system, and compared ϵ estimated by this method with that of integrating one-dimensional dissipation rate spectrum (Eq. (12)). Among others, Chen et al. [6] apply this method to characterize the turbulence using PIV measurements in a rapid straining turbulence facility.

When energy spectra are used to estimate ϵ, the raw PIV data must be preprocessed before fast Fourier transform (FFT) is applied to calculate the energy spectra: the ensemble mean velocity on every PIV node is subtracted; the obtained fluctuation velocity data are either detrended or windowed by employing different window functions. These preprocessing operations produce periodic signal sequences that are needed for FFT. Computing the integral in Eq. (12) using finite data sequence from PIV measurements introduces error caused by finite truncation in wavenumber space. ϵ determined from Eq. (14) is sensitive to the data points picked for

−5/3 curve fit. All these factors contribute to the uncertainty of measuring ϵ.

2.5. Estimate of ϵ from structure function

The second order velocity structure function

$$D_{ij}(\mathbf{r},t) \equiv \langle(u_i(\mathbf{x}+\mathbf{r},t) - u_i(\mathbf{x},t))(u_j(\mathbf{x}+\mathbf{r},t) - u_j(\mathbf{x},t))\rangle, \tag{15}$$

can be computed using PIV data measured at points $\mathbf{x}$ and $\mathbf{x}+\mathbf{r}$. For isotropic turbulence, in inertial subrange, the longitudinal structure function is related to of turbulent dissipation rate [13,20]

$$D_{LL}(r) \equiv D_{11}(r) = C_2(\epsilon r)^{2/3}, \tag{16}$$

where C_2 is a universal constant (C_2=2.12, as suggested by Sreenivasan [24]). This leads to another estimate of ϵ:

$$\epsilon = \frac{1}{r}\left(\frac{D_{LL}(r)}{C_2}\right)^{3/2}. \tag{17}$$

Jong et al. [12] apply this method to study a zero-mean isotropic turbulence. Different than the aforementioned energy spectra methods, this one does not apply FFT thus the aliasing associated with data preprocessing is less severe. In addition, analyzing the longitudinal structure function $D_{LL}(r)$ only needs velocity measurements along the longitudinal direction, which can be obtained by PIV without further assumptions about the other unresolved velocity gradient terms.

2.6. Issue of PIV resolution

In addition to the different methods for estimating ϵ, spatial resolution of PIV measurement also significantly impacts estimate of ϵ by influencing the accuracy of velocity gradient $\partial u_i'/\partial x_j$ [4]. This is because PIV measures an averaged velocity of all particles within a chosen interrogation window [21,1]. Thus the measured velocity represents a spatially filtered velocity (similar to the filtering operation in Large Eddy Simulation (LES) with interrogation window size as the characteristic size of the filter kernel) [23]. In Fig. 1, a filtering operation is applied to velocity field from a DNS dataset to demonstrate the effect of PIV resolution (represented by interrogation window size Δ). The DNS data (spatial resolution δ) are used to represent velocity field of uniformly distributed particles moving with the flow. The filtering operation results in significant underestimate of the magnitude of velocity gradient, thus causes significant error in the estimate of ϵ using these derivatives. Saarenrinne and Piirto [22] compare ϵ estimated from PIV data with the DNS results, and assert that the achieved PIV spatial resolution Δ is a critical factor in determining the accuracy of ϵ when $\Delta > \eta$ where η is smallest turbulent scale, Kolmogorov scale

$$\eta = (v^3/\epsilon)^{1/4}. \tag{18}$$

Lavoie et al. [14] introduce a correction method to ϵ estimated using PIV data, based on hotwire anemometry measurements, when Δ/η falls into a narrow range of 11−14. Tanaka and Eaton [27] introduce another correction method for cases when $\Delta < \eta$. Both methods need prior knowledge of η, which requires known value of ϵ according to Eq. (18).

3. Synthetic PIV velocity data from DNS data

In a PIV experiment, the fluid is seeded with small particles that follow the flow with a good fidelity. The particles in the sample volume are illuminated by a thin light sheet. Usually two consecutive images, with a controlled time interval, of the particles are recorded. In the PIV processing step, each particle image is divided into small subareas (interrogation windows), and a local
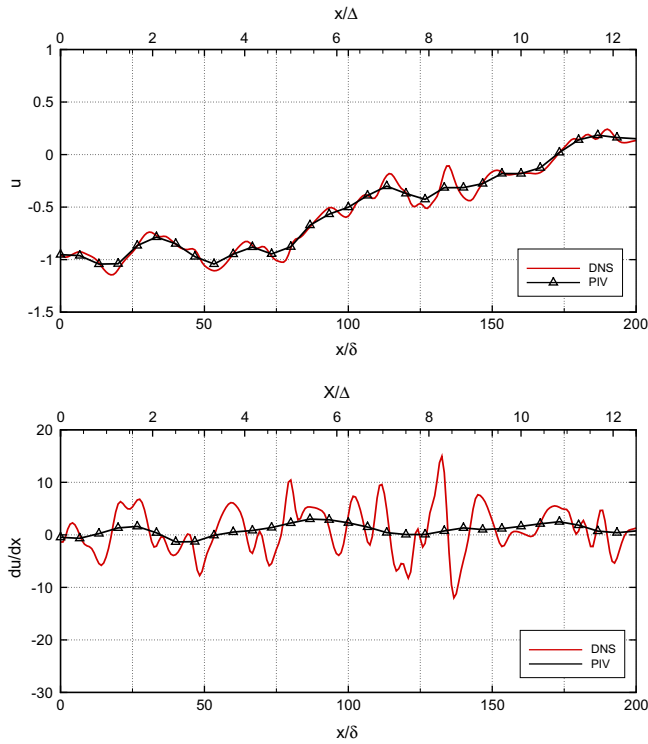
Fig. 1. Schematic illustration of PIV spatial resolution on computed velocity gradient. The PIV velocity sequence is generated by applying a one-dimensional (along x-direction) averaging filter ($\Delta = 16\delta$ and 50% overlap) to the DNS sequence. Plotted are distributions of non-dimensional velocity u (top) and non-dimensional velocity gradient $\partial u / \partial x$ (bottom).

displacement (thus local velocity) of each interrogation window is determined by tracking the motion of particle pattern within the interrogation window using a PIV processing algorithm (see [21,1] and therein references for details).

To quantify the accuracy of estimating ϵ using PIV data, we generate synthetic PIV data using a DNS dataset that has known value of ϵ. DNS solves the Navier–Stokes equations from the smallest scale (Kolmogorov scale) to the largest scale (turbulent integral length scale), without adopting a turbulent model. It has been applied to study physics of fluids (see, e.g., [18,20]). The DNS dataset used in this study is publicly accessible from *The JHU Turbulence Database Cluster* (http://turbulence.pha.jhu.edu/). It contains a total of 1024^3 points in a $[0, 2\pi]^3$ non-dimensional spatial domain and 1024 temporal samples spanning about one large-scale turnover time of isotropic forced turbulence (see Li et al. [16] for details). The corresponding non-dimensional spatial and temporal resolutions of the DNS dataset are $\delta = 0.006$ and $\delta_t = 0.002$, respectively. Characteristic parameters of this DNS dataset, including η and ϵ, are given in Table 1. The inertial subrange of this

Table 1
Characteristic parameters (non-dimensional) of the DNS data [16].

Kinematic viscosity, ν	0.000185
Total turbulent kinetic energy, E_t	0.695
Mean dissipation rate, ϵ	0.0928
rms velocity fluctuation, $u_{rms} = \sqrt{(2/3)E_t}$	0.681
Taylor micro scale, $\lambda = \sqrt{15\nu u_{rms}^2/\epsilon}$	0.118
Taylor-scale Reynolds number, $Re_\lambda = u_{rms}\lambda/\nu$	433
Kolmogorov time scale, $\tau_\eta = \sqrt{\nu/\epsilon}$	0.0446
Kolmogorov length scale, $\eta = (\nu^3/\epsilon)^{1/4}$	0.00287
Integral scale, L	1.376
Large eddy turnover time, $T_L = L/u_{rms}$	2.02

isotropic turbulent flow spans from 30η to 430η as estimated from radial kinetic energy spectrum ($-5/3$ curve, Fig. 2, [16]). The values of parameters given in Table 1 serve as true values and will be compared with the ones computed using synthetic PIV data.

The synthetic PIV velocity data are generated in a procedure as shown in Fig. 2: (a) seeding particles, with an averaged diameter three pixel and particle density 0.01 particle per pixel (these optimal values are suggested in [21]), are randomly distributed in the test section simulated by a DNS snapshot at a time instance t_1; the diameter and scattered light intensity of each particle are determined using a Gaussian distribution; (b) the velocity of each particle is determined by bi-cubic interpolation of the DNS velocity data around each particle location at t_1; (c) with a given time interval, Δt, each particle moves to a new location at a time instance $t_2 = t_1 + \Delta t$; (d) the grayscale image of each particle is described by a Gaussian function of its diameter, and the synthetic image is obtained by overlying the grayscale of all particles in the recording plane; and (e) a cross-correlation based PIV algorithm is applied to the image pair to retrieve measured velocities. In this process, both the top-hat and Gaussian weighted (circular) interrogation windows are applied to quantify the effects of different windows [1]. One may refer to Lecordier et al. [15], Westerweel et al. [29] and Gui and Wereley [9] and therein references for complete details of generating synthetic PIV images. The velocity data obtained in this approach (denoted as $\widetilde{u}_i^\Delta$) are categorized as *Synthetic-PIV-Dataset* in this paper.

Since different particles within a same interrogation window have different velocities (u_i), the velocity measured by PIV represents a filtered velocity of all particles within the interrogation window (Fig. 3), modeled by a two-dimensional filtering operation:

$$\bar{u}_i^\Delta = u_i \otimes G_\Delta, \tag{19}$$

where G_Δ is the filtering kernel, representing the operation of PIV interrogation algorithm on velocity field of individual particles to extract the local velocity of each interrogation window, and $\otimes$ represents a convolution operator. With this understanding, synthetic PIV velocity fields can be also obtained by filtering the velocities of all particles within an interrogation window without generating synthetic PIV images. When a 2D top-hat filter of size $\Delta_x \times \Delta_y$ is used, the velocity measured by PIV is a spatially averaged value of all particle velocities within the interrogation window [21], i.e.,

$$\bar{u}_i^\Delta(x_1, x_2, t) = \frac{1}{\Delta_x \Delta_y} \iint_\infty u_i(x_1 - s_1, x_2 - s_2) \cdot H\left(\frac{1}{2} - \frac{|s_1|}{\Delta_x}\right)$$
$$\cdot H\left(\frac{1}{2} - \frac{|s_2|}{\Delta_y}\right) ds_1\, ds_2, \tag{20}$$

where H is Heaviside function. Thus $\bar{u}^\Delta$ represents another model of generating synthic PIV velocity from DNS data, and it is denoted as *Filtered-PIV-Dataset* in this paper. As in most PIV processing, we choose the interrogation window of square shape ($\Delta_x = \Delta_y = \Delta$) and evaluate the integral digitally.

Synthetic PIV data ($\widetilde{u}_i^\Delta$ and $\bar{u}_i^\Delta$) with different interrogation window sizes can be generated using the same DNS dataset by varying Δ. Here Δ ranges from 2η to 60η, which falls into the universal equilibrium range (dissipation range and inertial subrange) of the DNS dataset. We retrieve 500 velocity snapshots from particle images (1024×160 pixels) for the analysis in the present study. For each snapshot, both top-hat filter and Gaussian filter are applied, corresponding to the top-hat and Gaussian weighted interrogation windows in cross correlation, respectively.

Furthermore, two-dimensional histograms of ($\widetilde{u}_i^\Delta, \bar{u}_i^\Delta$) from all synthetic PIV data (Fig. 4) reveal a strong linear correlation between $\widetilde{u}_i^\Delta$ and $\bar{u}_i^\Delta$ for different window types (top-hat and Gaussian) and window sizes (Δ). This suggests that the output of cross
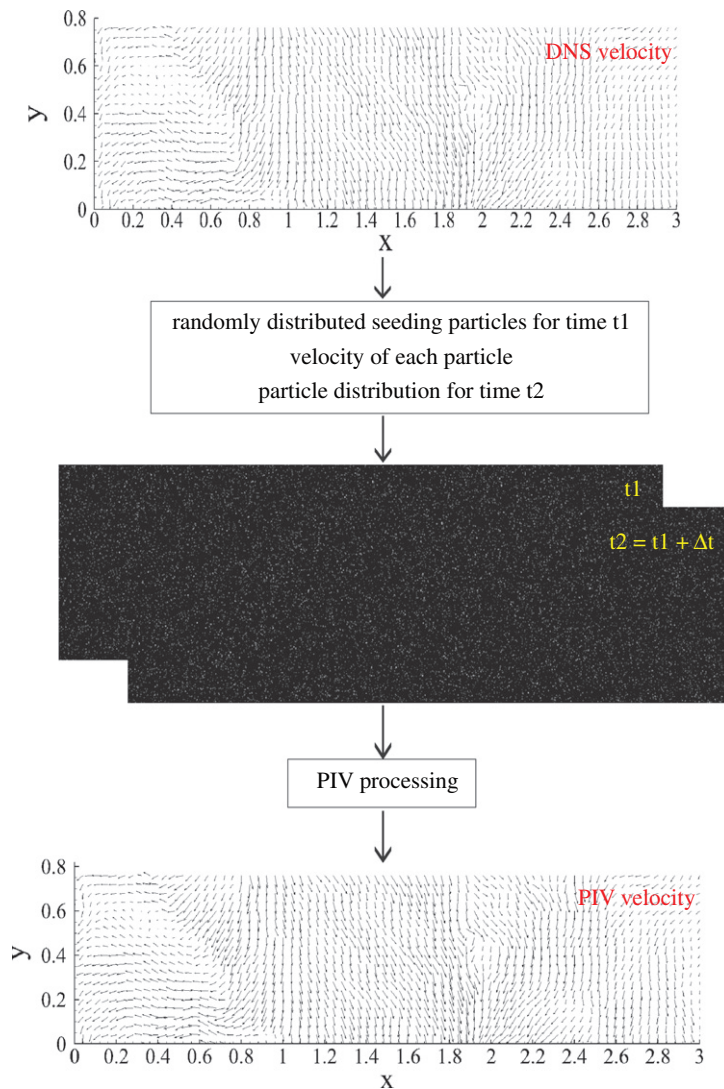
Fig. 2. Schematic illustration of generating a PIV velocity map by synthetic images. To be noted: every other eight vector is plotted here for clear display.
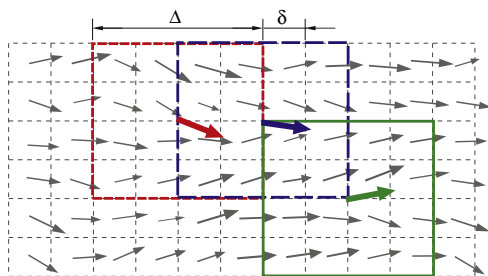

Fig. 3. Schematic illustration of synthetic PIV velocity vectors (red, blue and green arrows) represent averaged velocity of $N \times N$ ($N = 4$ in this figure) uniformly seeded particles (gray vectors) in the interrogation window (size $\Delta = N \cdot \delta$, red, blue and green squares, respectively), with 50% window overlap. (For interpretation of the references to color in this figure legend, the reader is referred to the web version of this article.)

correlation based PIV process can be also mathematically described by a filter operation (Eqs. (19) and (20)). The primary advantage of utilizing *Filtered-PIV-Dataset* is that only windowing effect exists, without contamination of other error sources from synthetic particle generation and PIV algorithm, such as subpixel interpolation, particle seeding density, and peak locking.

4. Estimate of ϵ using synthetic PIV data

Both synthetic PIV datasets are used to estimate ϵ by employing isotropy assumption (Eq. (5)), local axisymmetry assumption (Eq. (6)) and local isotropy assumption (Eq. (9)), i.e., substituting $u_i(\mathbf{x}, t)$ with $\widetilde{u}_i^A(\mathbf{x}, t)$ or $\bar{u}_i^A(\mathbf{x}, t)$ in these three equations. The computed turbulent dissipation rate is denoted as ϵ_m (to differentiate from the true value ϵ). One is reminded that the velocity fluctuations in these equations are first computed by subtracting ensemble averaged mean velocity, $\langle \widetilde{u}^A \rangle$ or $\langle \bar{u}^A \rangle$, from instantaneous velocity, $\widetilde{u}_i^A(\mathbf{x}, t)$ or $\bar{u}_i^A(\mathbf{x}, t)$, in the data processing step. The velocity gradients are computed using 5-point central difference scheme. In addition, when Eq. (6) is applied in the present study, the local axisymmetry is chosen with respect to x_1. Furthermore, the energy spectra method (Eq. (14)) and the structure function method (Eq. (17)) are also applied to the synthetic PIV data to estimate ϵ. Fig. 5 shows the measured values of turbulent dissipation rate (ϵ_m) normalized by the true value of ϵ, as a function of normalized interrogation window size Δ/η. ϵ_m based on calculation of spatial gradients of velocity fluctuation ("isotropy", "local axisymmetry" and "local isotropy" methods) decreases significantly as Δ increases. For instance, when $\Delta > 20\eta$, $\epsilon_m/\epsilon < 3\%$. However, ϵ_m calculated using the structure function method or energy spectra

method decreases relatively slowly as Δ increases. At $\Delta = 50\eta$, ϵ_m is still about $20-30\%$ of its corresponding true value. The observed differences are due to the fact that accuracies of the first three methods are deteriorated by the underestimated velocity gradients at large PIV resolutions. The accuracies of the structure function method and spectra method are dependent on $\bar{u}_i^\Delta$ (rather than velocity gradient $\partial \bar{u}_i^\Delta / \partial x_j$), thus the smoothing effect of the filtering operation (Eq. (19)) is less severe. In addition, the structure function method and energy spectra method can be applied to any turbulent flow that falls into the category of Kolmogorov similarity hypothesis, where inertial subrange and dissipation range display universal statistical characteristics.

5. Correction methods of dissipation rate estimate using PIV data

The turbulent dissipation rates calculated directly using velocity gradients (Eqs. (5), (6), and (9)) display large errors when the interrogation window size is larger than Kolmogorov scale. In these three methods, assumptions are needed to appropriately model the unresolved velocity gradient terms (Eq. (3)). In this section, we focus on the other two methods (structure function method and energy spectra method) and explore improvement of these two methods.

5.1. Modified Structure Function Method

The longitudinal structure function can be calculated from Eq. (15) using DNS data:

$$D_{LL}(r) = \langle (u_1(x+r) - u_1(x))^2 \rangle. \tag{21}$$
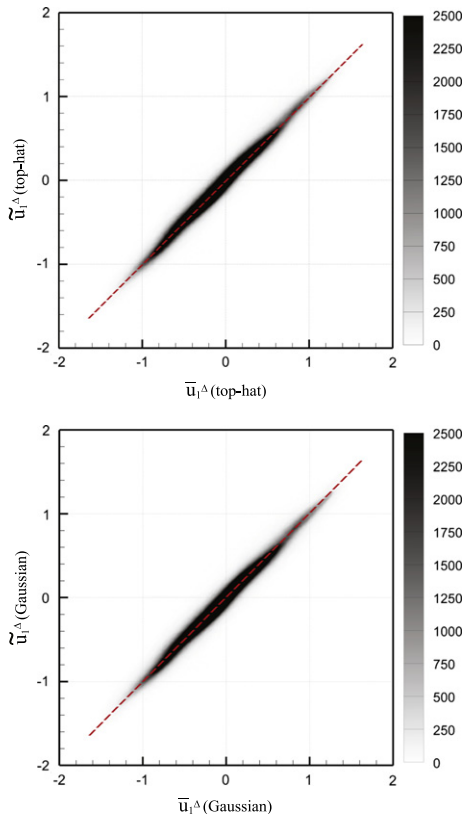
Fig. 4. Two-dimensional histograms representing the correlation between $\widetilde{u_1}^\Delta$ and $\bar{u}_1^\Delta$ ($\Delta = 8\delta$) generated from filter operation and synthetic PIV procedure. (Top) is from top-hat filter and top-hat interrogation window, and (bottom) is from Gaussian filter and Gaussian interrogation window. Dash lines mark the 45° slope.

When velocity field from PIV measurement is used, we get a measured value of $D_{LL}(r)$:

$$D_{LL}^m(r) = \left\langle \left(\widetilde{u}_1^\Delta(x+r) - \widetilde{u}_1^\Delta(x) \right)^2 \right\rangle. \tag{22}$$

where superscript "m" denotes the value using PIV data. By applying Eq. (19), one can further have

$$D_{LL}^m(r) = \left\langle \left((u_1(x+r) - u_1(x)) \otimes G_\Delta \right)^2 \right\rangle = f(D_{LL}(r), \Delta). \tag{23}$$

This suggests that $D_{LL}^m(r)$ depends on the interrogation window size for a given filtering kernel. As shown in Fig. 6, $D_{LL}^m(r)$ decreases as Δ increases in the inertial subrange and dissipation range. As a result, a Δ-dependence exists for ϵ_m determined from $D_{LL}^m(r)$ using the structure function method, i.e.,

$$\epsilon_m = g(D_{LL}, \Delta). \tag{24}$$

According to Kolmogorov's similarity hypothesis, in the inertial subrange and dissipation range, the statistics of small-scale motions (e.g., $D_{LL}(r)$) have a universal form. As a result, for a given filtering kernel G, the Δ-dependence of the ϵ_m/ϵ can be established empirically by examining the synthetic PIV data in the inertial subrange and dissipation range.

The *Filtered-PIV-Dataset* from top-hat and Gaussian (standard deviation $\sigma = \Delta/4$) filter operations, as well as *Synthetic-PIV-Dataset*, with different Δ's are applied to test this. As mentioned before, these two filter operations represent uniform averaging and Gaussian weighted averaging of particle velocities within interrogation window, respectively, corresponding to the uniform interrogation window and Gaussian interrogation window, as introduced in Adrian and Westerweel [1]. Using these data, $D_{LL}^m(r)$ is computed from Eq. (23) and then ϵ_m is determined by Eq. (17). The results are shown in Fig. 7. It is evident that these two filtering operations (i.e., different averaging within interrogation window) result in difference in estimate of ϵ even at same Δ, which represents different windowing effects. With the same Δ, ϵ_m's from *Filtered-PIV-Dataset* and *Synthetic-PIV-Dataset* coincide well, which is both observed in top-hat and Gaussian window results, and this confirms the validity of *Filtered-PIV-Dataset* again. Furthermore, two-term exponential curves best fit the experiment data in Fig. 7 and thus empirical relationships between ϵ_m/ϵ and Δ/η can be established,

$$\frac{\epsilon_m}{\epsilon} = \alpha_1 \exp\left(\alpha_2 \cdot \frac{\Delta}{\eta} \right) + \beta_1 \exp\left(\beta_2 \cdot \frac{\Delta}{\eta} \right), \tag{25}$$

where the coefficients α_i and β_i ($i = 1, 2$) are given in Table 2. Both curves give $\epsilon_m \to \epsilon$ as $\Delta \to \eta$. In the process of establishing these
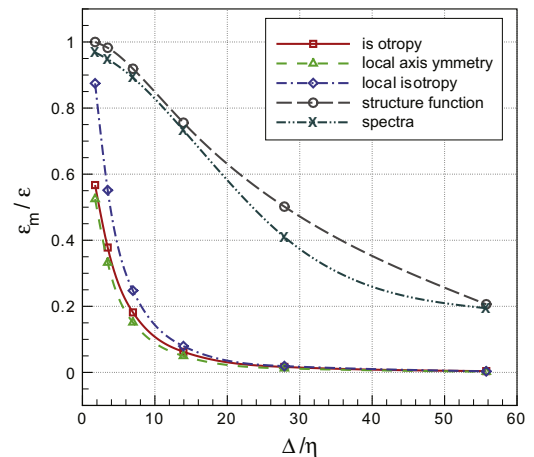
Fig. 5. Comparison of measured values of turbulent dissipation rate (ϵ_m) using $\bar{u}_i^\Delta$ with different Δ. Legend: isotropy (Eq. (5)), axisymmetry (Eq. (6)), local isotropy (Eq. (9)), energy spectra (Eq. (14)), and structure function (Eq. (17)).
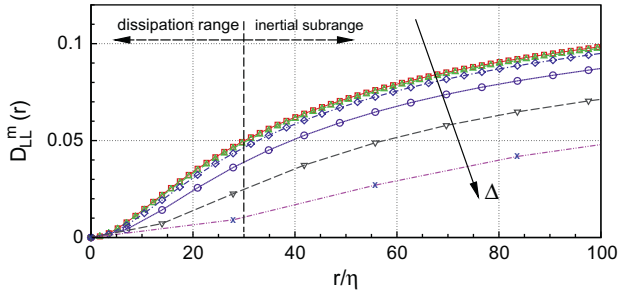
Fig. 6. $D_{LL}^m(r)$ computed using synthetic PIV data at different interrogation window sizes. Values of Δ/η for different curves: 1, 2, 4, 8, 16 and 32.
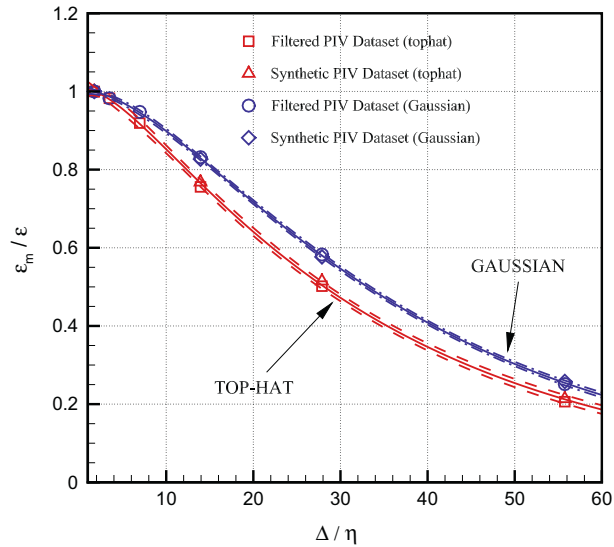

Fig. 7. ϵ_m calculated using the structure function method as a function of interrogation window size Δ. The PIV data are generated through applying top-hat and Gaussian filters, as well as synthetic PIV procedure using top-hat and Gaussian interrogation windows. Solid curves show the fitted curves in Eq. (25), and dash (dash dot) curves show the 95% confident intervals of the fitted curves.

Table 2
Coefficients in Eq. (25).

Window type	α_1	α_2	β_1	β_2
Top-hat	+1.1910	−0.03081	−0.1835	−0.2062
Gaussian	+1.2670	−0.02795	−0.2737	−0.1545

relationships, ϵ_m and Δ are unknown variables while ϵ and η are used as known parameters from DNS. However, in practical application, Δ is of a given value and ϵ_m can be estimated using PIV data, while ϵ and η are the variables need to be determined. Using ϵ and η as normalization parameters is also because another relation between ϵ_m/ϵ and Δ/η can be derived directly from the definition (18), such as:

$$\frac{\epsilon_m}{\epsilon} = \left(\frac{\epsilon_m \Delta^4}{\nu^3}\right)\left(\frac{\Delta}{\eta}\right)^{-4}, \tag{26}$$

to close the equations. From Eq. (25) (obtained by examining the synthetic PIV data) and (26) (from analyzing a specific PIV measurement), the true values of ϵ and η can be solved (cross point in Fig. 8). We name this approach *Modified Structure Function Method*.

One is reminded that for a given filtering kernel G_Δ (corresponding to a different PIV interrogation algorithm) there will be a different set of coefficients in Eq. (25). This empirical relationship
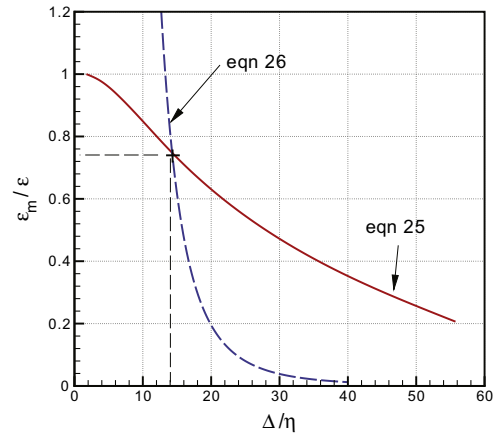

Fig. 8. Determining ϵ and η from Eqs. (25) and (26), using Δ and measured value ϵ_m.
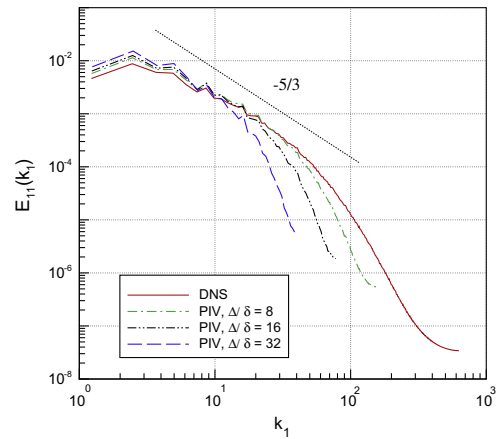

Fig. 9. $\widetilde{E}_{11}(k_1)$ computed using PIV data at different interrogation window sizes.

between ϵ_m/ϵ and Δ/η must be aforehand established using synthetic PIV data, as described in this paper for 2D top-hat filter or Gaussian filter. In addition, this correction routine is rooted on Kolomogorov's similarity hypothesis. To apply this approach, interrogation window size Δ should fall into the range of dissipation range or inertial subrange. This can be checked afterwards by comparing Δ to η. Since square-shape uniform interrogation window is mostly used in PIV process, in the following discussion, we focus on data from 2D top-hat filter.

5.2. Modified Spectra Method

As mentioned previously, the PIV correlation procedure can be modeled as a filter operation to the motions of particles within the interrogation window. Thus, the longitudinal energy spectra $\widetilde{E}_{11}(k_1)$ and $E_{11}(k_1)$, computed using PIV velocity data $\bar{u}_i^\Delta$ and true velocity u_i, respectively, have a relationship

$$\widetilde{E}_{11}(k_1) = |\widehat{G}(k_1)|^2 E_{11}(k_1), \tag{27}$$

where $\widehat{G}(k_1)$ is the Fourier transform of the filter kernel G (similar to the relationship in large eddy simulation, see, e.g., [20]). Thus, with $\widetilde{E}_{11}(k_1)$ computed using PIV data, the true longitudinal energy spectrum can be obtained by:

$$E_{11}(k_1) = \frac{\widetilde{E}_{11}(k_1)}{|\widehat{G}(k)|^2}. \tag{28}$$
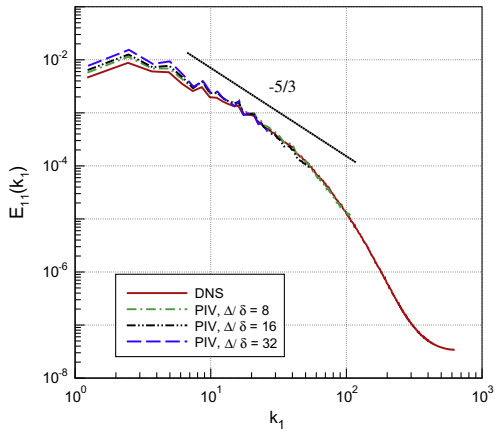
Fig. 10. $E_{11}(k_1)$ computed using Eq. (28) at different interrogation window sizes.
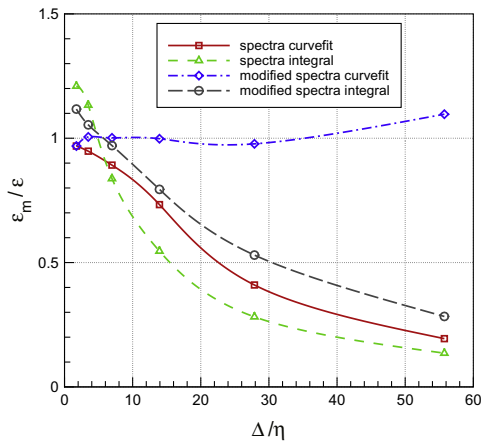

Fig. 11. The turbulent dissipation rate calculated based on the spectra methods.

The curves for $\widetilde{E}_{11}(k_1)$ and corresponding $E_{11}(k_1)$ using *Filtered-PIV-Dataset* at different Δ's are given in Figs. 9 and 10. A $-5/3$ slope is also show to identify the inertial subrange. Applying Eq. (28) leads to a converged estimate of $E_{11}(k_1)$ within the resolvable range of k_1 using PIV data at different interrogation window sizes. As introduced in the Section 2, ϵ can then be estimated from this $E_{11}(k_1)$ by applying spectra integral method (Eq. (12)) or spectra curvefit method (Eq. (13)). In this paper, this two approaches (using $E_{11}(k_1)$ obtained from $\widetilde{E}_{11}(k_1)$) are titled *Modified Spectra Integral Method* and *Modified Spectra Curvefit Method*, respectively.

Fig. 11 shows the turbulent dissipation rates estimated by the aforementioned energy spectra methods (original and modified) using *Filtered-PIV-Dataset* at different interrogation window sizes. The integrals are evaluated using $\widetilde{E}_{11}(k_1)$ or $E_{11}(k_1)$ on all resolvable k_1 range with a trapeziform scheme, whereas the curvefit is applied to data from an identified inertial subrange by matching the $-5/3$ slope. Both integral methods demonstrate decreasing trend of the estimated values of ϵ as Δ increases. The Modified Spectra Integral Method does not demonstrate significant superiority. Another noticeable issue is that the two integral methods also give overpredicted values ($\epsilon_m > \epsilon$) when $\Delta/\eta < 4$. These errors are possibly caused by the facts that the spectra integral methods need accurate values of the spectra, in particular, at low wavenumber range (energy-containing and flow-specific) and the results are sensitive to numerical integration scheme and wavenumber truncation in this range. On the other hand, the Modified Spectra Curvefit Method successfully gives an estimate of the turbulent

dissipation rate close to the true value. Certain overprediction is observed at large interrogation window sizes (about 10% at $\Delta/\eta = 55$).

6. Applications on experimental PIV data

The aforementioned methods for estimating ϵ, including the ones reviewed in Section 2 and the modified methods proposed in Section 5, are applied to PIV data acquired in a turbulent jet experiment. As shown in Fig. 12, the experimental facility is composed of a main tank and a jet nozzle. The main tank, of dimensions of $110 \times 30 \times 25$ cm^3, is made of 1.27 cm thick acrylic plates, and is filled with water. The jet nozzle is designed to generate a stable flow profile at the nozzle exit, with an inside diameter of $D = 1.27$ cm. The jet nozzle is manufactured by 3D jet printing technique, and is connected to a constant head system (not shown in Fig. 12, composed of a head-control tank, a supply tank and two circulating pumps) by a pump to introduce a round jet into the main tank. Details of the facility can be found in Xu and Chen [30]. The origin of the coordinate system is set at the center of the jet exit plane. x-axis (x_1) is set horizontally along the flow direction. y-axis (x_2) is set to be perpendicular to the x-axis in the horizontal plane. z-axis (x_3) points upwardly and is antiparallel to gravitational direction. For the data used in this paper, the initial injection velocity at nozzle exit is $U = 1.9$ m/s. The turbulent intensity and Reynolds number are $u'/U \simeq 3.3\%$ and $Re = \rho UD/\mu = 24,000$, respectively. The water is uniformly seeded with hollow glass beads (median diameter 11 μm, specific gravity 1.1) for PIV measurement. A twin-head Nd:YAG pulse laser (532 nm, peak energy 130 mJ/pulse) illuminates the test section by forming a 1 mm thick laser sheet though a group of optics. A CCD camera (14-bit Imager ProX 4M camera) of 2112×2072 pixels resolution records particle images, operated under double exposure mode at a sampling rate of 5 Hz. The time delay between the two pulses is set to 600 μs. Velocity vectors are retrieved by processing image pairs using PIV analysis software (Davis 7.0). The PIV images used in the present paper are recorded in the central vertical x–z plane ($y = 0$), at downstream range of $x/D = 16$–24. One-dimensional kinetic energy spectra, $E_{11}(k_1)$ and $0.75E_{33}(k_1)$ are shown in Fig. 13. The collapse of these two curves in inertial subrange manifests the isotropy of the turbulence. Top-hat interrogation window (equivalent spatial size Δ) is used in each processing. Multiple values of Δ are chosen to process the same group of PIV images to obtain $\widetilde{u}_i^{\Delta}(x_1, x_3)$ ($i = 1, 3$). For the data reported here, the interrogation window sizes are $16 \times 16, 32 \times 32$, and 64×64 pixels, with 50% overlap, corresponding to $\Delta = 0.88, 1.75$ and 3.50 mm, respectively. 600 velocity snapshots are analyzed for obtaining statistically-convergent results. The PIV data at different window sizes ($\widetilde{u}_i^{\Delta}(\mathbf{x}, t)$) are then used to estimate the dissipation rate by applying the aforementioned methods including *Modified Spectra Curvefit Method* and *Modified Structure Function Method*. In particular, when local axisymmetry assumption (Eq. (6)) is employed, x_1 is selected as the axisymmetric axis. The structure function ($D_{LL}^m(r)$) and energy spectra ($\widetilde{E}_{11}(k_1)$) are computed along x direction using data in range $0 < z/D < 2$. The values of ϵ_m from different methods (averaged over the area of interest: $16 \leqslant x/D \leqslant 24$ and $0 \leqslant z/D \leqslant 2$) are given in Tables 3 and 4. Results of different methods are further compared in Fig. 14. ϵ_m from the first three methods is significantly underestimated. This also lead to the overestimate of Kolmogorov scales. The general trends as function of interrogation window size qualitatively agrees with the ones observed from synthetic PIV data (Fig. 5). The two modified methods give nearly converged estimate of ϵ at different interrogation window sizes. This demonstrates a promising improvement of the dissipation rate estimated from these two methods when applied to
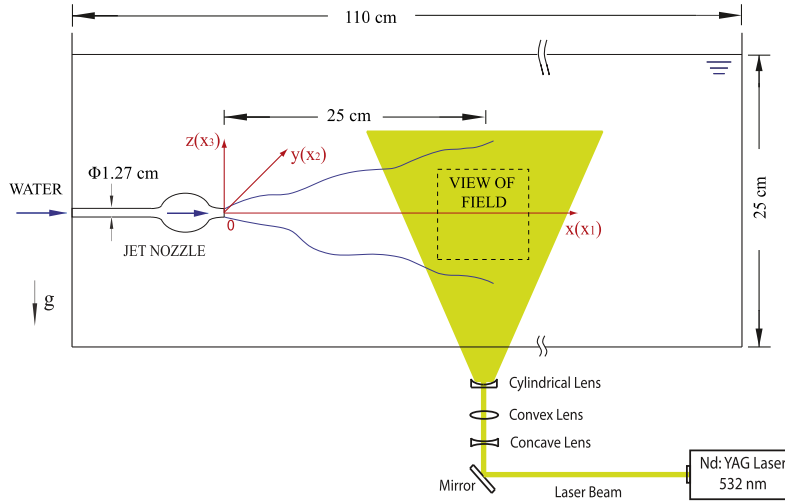
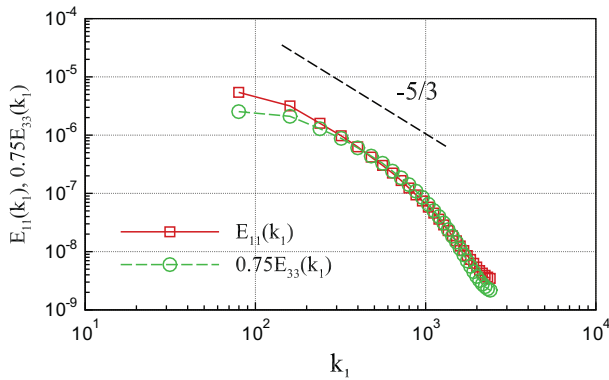**Fig. 12.** Schematic of the turbulent round jet experiment.

Fig. 13. One-dimensional kinetic energy spectra, $E_{11}(k_1)$ and $0.75E_{33}(k_1)$, of the turbulent jet.

Table 3
The turbulent dissipation rate and Kolomogorov scale estimated using PIV data.

Method	Interrogation window	ϵ_m (m²/s³)	η_m (m)
Isotropy (Eq. (5))	16 Pixel ($\Delta = 0.88$ mm)	1.49×10^{-2}	9.08×10^{-5}
	32 Pixel ($\Delta = 1.75$ mm)	5.77×10^{-3}	1.15×10^{-4}
	64 Pixel ($\Delta = 3.50$ mm)	1.93×10^{-3}	1.51×10^{-4}
Local axisymmetry (Eq. (6))	16 Pixel ($\Delta = 0.88$ mm)	1.30×10^{-2}	9.39×10^{-5}
	32 Pixel ($\Delta = 1.75$ mm)	4.87×10^{-3}	1.20×10^{-4}
	64 Pixel ($\Delta = 3.50$ mm)	1.56×10^{-3}	1.59×10^{-4}
Local isotropy (Eq. (9))	16 Pixel ($\Delta = 0.88$ mm)	2.12×10^{-2}	8.31×10^{-5}
	32 Pixel ($\Delta = 1.75$ mm)	7.99×10^{-3}	1.06×10^{-4}
	64 Pixel ($\Delta = 3.50$ mm)	2.59×10^{-3}	1.41×10^{-4}
Spectra curvefit (Eq. (14))	16 Pixel ($\Delta = 0.88$ mm)	9.00×10^{-2}	5.79×10^{-5}
	32 Pixel ($\Delta = 1.75$ mm)	6.48×10^{-2}	6.29×10^{-5}
	64 Pixel ($\Delta = 3.50$ mm)	5.43×10^{-2}	6.57×10^{-5}
Structure function (Eq. (17))	16 Pixel ($\Delta = 0.88$ mm)	7.16×10^{-2}	6.13×10^{-5}
	32 Pixel ($\Delta = 1.75$ mm)	4.88×10^{-2}	6.75×10^{-5}
	64 Pixel ($\Delta = 3.50$ mm)	1.91×10^{-2}	8.54×10^{-5}

experimental data. Combining the results from these two modified methods at three window sizes gives $\epsilon = (1.05 \pm 0.09) \times 10^{-1}$ m²/s³ and $\eta = (5.58 \pm 0.11) \times 10^{-5}$ m, respectively. As a result, the three interrogation window sizes are 15.8η, 31.4η, and 62.7η, respectively, in Table 4. These ratios suggests that chosen Δ's are within the inertial subrange or dissipation range, as required by both modified methods.

The Modified Structure Function and Modified Spectra Curvefit Methods can achieve an improved estimate the global turbulent dissipation rate than the traditional methods mentioned in Section 1, but the velocity-gradient methods (Eqs. (5), (6), and (9)) indeed have their advantages to capture the local variation of ϵ, although they have limitations (as mentioned in Sections 1 and 4). Here we present a correction for estimating ϵ using these methods:

$$\epsilon_g(x, y) = \beta_\Delta \cdot \epsilon_{g,m}(x, y), \qquad (29)$$

where $\epsilon_{g,m}(x, y)$ is the local dissipation estimated by velocity-gradient method, and $\epsilon_g(x, y)$ is the corrected local dissipation using velocity-gradient method. And the correction coefficient, β_Δ, is a function of Δ and defined as:

$$\beta_\Delta = \frac{\langle \epsilon \rangle}{\langle \epsilon_{g,m} \rangle}, \qquad (30)$$

where $\langle \epsilon \rangle$ and $\langle \epsilon_{g,m} \rangle$ are the averaged dissipation using Modified Structure Function Method (or Modified Spectra Curvefit Method)

and velocity-gradient methods, respectively, for a selected area. As shown in Fig. 15, ϵ_g reveals the spatial variation of ϵ with improved accuracy.

7. Conclusion

Quantifying the turbulent dissipation rate provides insight into the physics of the turbulent flows. However, the accuracy of estimating turbulent dissipation rate using planar PIV velocity data is affected by the way of modeling the unresolved velocity gradient terms and the PIV spatial resolution. In this paper, we first give a brief review of different methods used to estimate ϵ using PIV data. To validate the effectiveness of different methods, we follow the usual method to generate synthetic PIV images from a turbulence DNS dataset (with known ϵ) to obtain synthetic PIV velocity with different interrogation window sizes. Based on the fundamental mechanism of PIV, *Filtered-PIV-Dataset* is also generated through filtering operations to the same DNS dataset with different Δ's. Two-dimensional histograms are shown to validate modeling the correlation process in PIV processing using filtering operation. Direct estimate of ϵ using velocity gradients, with the assumption of

Table 4
Results of two modified methods.

| Method	Interrogation window	ϵ (m²/s³)	η (m)
Modified Spectra Curvefit	16 Pixel ($\varDelta = 0.88$ mm)	1.11×10^{-1}	5.50×10^{-5}
	32 Pixel ($\varDelta = 1.75$ mm)	1.00×10^{-1}	5.64×10^{-5}
	64 Pixel ($\varDelta = 3.50$ mm)	9.48×10^{-2}	5.72×10^{-5}
Modified Structure Function	16 Pixel ($\varDelta = 0.88$ mm)	9.77×10^{-2}	5.67×10^{-5}
	32 Pixel ($\varDelta = 1.75$ mm)	1.09×10^{-1}	5.52×10^{-5}
	64 Pixel ($\varDelta = 3.50$ mm)	1.17×10^{-1}	5.43×10^{-5}

isotropy, local axisymmetry, or local isotropy, gives significant underestimated values as interrogation window size increases. On the other hand, the indirect estimation of ϵ from energy spectra
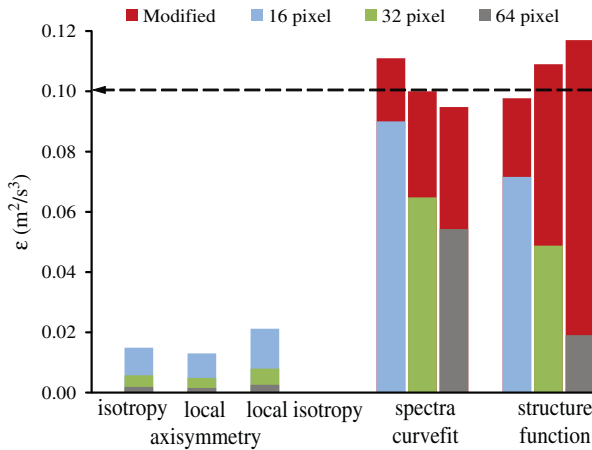
Fig. 14. Comparison of ϵ estimated from different methods. Dash line gives averaged value of ϵ from modified methods.

and structure function demonstrate less severe decrease as $\varDelta$ increases. We analyze the influence of $\varDelta$ on computing energy spectra and structure function and propose two modified methods. The *Modified Structure Function Method* relies on an empirical relationship between ϵ_m/ϵ and $\varDelta/\eta$ that is established using synthetic PIV data. For a measured value ϵ_m at given $\varDelta$, the true values of ϵ and η can be solved from this relationship. The *Modified Spectra Method* accounts the averaging effect introduced by the interrogation window and thus gives a better calculation of the energy spectra. When the new spectra are used to curve fit the $-5/3$ slope, an improved estimate of ϵ is expected. When these two methods are applied to experimental PIV dataset acquired from a turbulent jet experiment, they yield nearly converged estimates of turbulent dissipation rate and Kolmogorov scale at different interrogation window sizes. This suggests that these two methods overcome the $\varDelta$-dependence owned by other methods. Using the ϵ determined by these two methods, a correction coefficient $\beta_\varDelta$ can be introduced in other three direct methods to improve the accuracy of the local values of ϵ.

One is reminded that the two modified methods can be applied to isotropic turbulent flows which fall into the framework of Kolmogorov's similarity hypothesis, where inertial subrange and dissipation range display universal statistical characteristics. When the turbulence displays a strong anisotropy or non-homogeneity, the effectiveness of the modified methods should be further validated, e.g., by DNS dataset with known true value. The existence of strong mean rotation or mean shear motion within the interrogation window is not explored in the present study due to lack of access to such DNS dataset. The modified methods require that the interrogation window size is within the inertial subrange or dissipation range. This prerequisite should be re-checked with Kolmogorov scale obtained from the modified methods. Furthermore, different pre-treatment of the interrogation window should also be addressed differently when these two modified methods
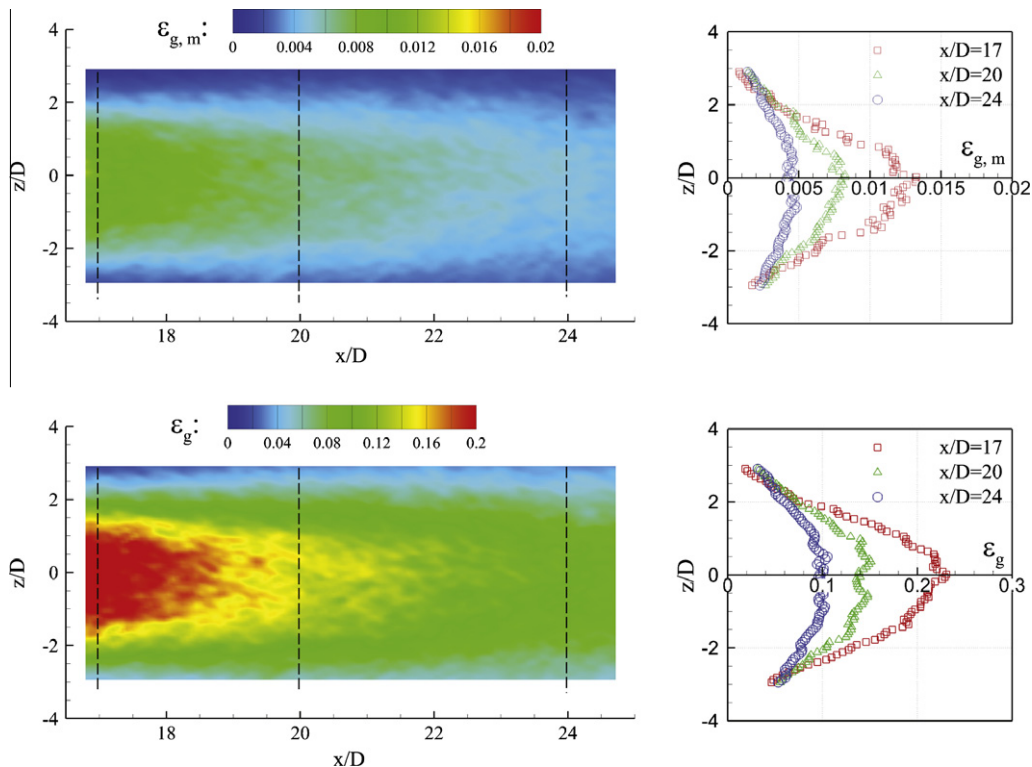
Fig. 15. Contour and profile comparison of ϵ_g and $\epsilon_{m,g}$ of experimental PIV data using local isotropic assumption without (top) and with $\beta_\varDelta$ correction (bottom). To be noted: the maximum contour level and x-axis maximum limit for bottom plots are 10 times of those for the top plots.

are applied. The influences of these factors should be explored in future studies.

References

[1] R.J. Adrian, J. Westerweel, Particle Image Velocimetry, Cambridge University Press, 2010.
[2] R.A. Antonia, J. Kim, L.W.B. Browne, Some characteristics of small-scale turbulence in a turbulent duct flow, J. Fluid Mech. 233 (1991) 369–388.
[3] R.A. Antonia, B.R. Pearson, Effect of initial conditions on the mean energy dissipation rate and the scaling exponent, Phys. Rev. E 62 (6) (2000) 8086–8090.
[4] R.A. Antonia, Y. Zhu, J. Kim, On the measurement of lateral velocity derivatives in turbulent flows, Exp. Fluids 15 (1993) 65–69.
[5] P. Burattini, P. Lavoie, R.A. Antonia, On the normalized turbulent energy dissipation rate, Phys. Fluids 17 (9) (2005) 098103.
[6] J. Chen, C. Meneveau, J. Katz, Scale interactions of turbulence subjected to a straining–relaxation–destraining cycle, J. Fluid Mech. 562 (2006) 123–150.
[7] P. Doron, L. Bertuccioli, J. Katz, T.R. Osborn, Turbulence characteristics and dissipation estimates in the coastal ocean bottom boundary layer from PIV data, J. Phys. Oceanogr. 31 (2001) 2108–2134.
[8] W.K. George, H.J. Hussein, Locally axisymmetric turbulence, J. Fluid Mech. 233 (1991) 1–23.
[9] L. Gui, S.T. Wereley, A correlation-based continuous window-shift technique to reduce the peak-locking effect in digital PIV image evaluation, Exp. Fluids 32 (2002) 506–517.
[10] J.O. Hinze, Turbulence, McGraw-Hill, New York, 1975.
[11] J.O. Hinze, Turbulence, An Introduction to Its Mechanism and Theory, McGraw-Hill, Toronto, 1987.
[12] J. Jong, L. Cao, S. Woodward, J. Salazar, L. Collins, H. Meng, Dissipation rate estimation from PIV in zero-mean isotropic turbulence, Exp. Fluids 46 (2009) 499–515.
[13] A.N. Kolmogorov, Dissipation of energy in locally isotropic turbulence, Dokl. Akad. Nauk SSSR 32 (1941) 19–21 (in Russian).
[14] P. Lavoie, G. Avallone, F.D. Gregorio, G. Romano, R. Antonia, Spatial resolution of PIV for the measurement of turbulence, Exp. Fluids 43 (2007) 39–51.
[15] B. Lecordier, D. Demare, L.M.J. Vervisch, J. Réveillon, M. Trinité, Estimation of the accuracy of PIV treatments for turbulent flow studies by direct numerical simulation of multi-phase flow, Meas. Sci. Technol. 12 (2001) 1382–1391.
[16] Y. Li, E. Perlman, M. Wan, Y. Yang, C. Meneveau, R. Burns, S. Chen, A. Szalay, G. Eyink, A public turbulence database cluster and applications to study lagrangian evolution of velocity increments in turbulence, J. Turb. 1–29 (31) (2008) 539–578.
[17] J.L. Lumley, Some comments on turbulence, Phys. Fluids A: Fluid Dyn. 4 (2) (1992) 203–211.
[18] P. Moin, K. Mahesh, Direct numerical simulation: a tool in turbulence research, Annu. Rev. Fluid Mech. 30 (1998) 539–578.
[19] A. Monin, A. Yaglom, Statistical Fluid Mechanics: Mechanics of Turbulence, vol. 2, The MIT Press, 1975.
[20] S.B. Pope, Turbulent Flows, Cambridge University Press, Cambridge, 2001.
[21] M. Raffel, C. Willert, S. Wereley, J. Kompenhans, Particle Image Velocimetry – A Practical Guide, second ed., Springer, 2007.
[22] P. Saarenrinne, M. Piirto, Turbulent kinetic energy dissipation rate estimation from PIV velocity vector fields, Exp. Fluids 29 (Suppl.) (2000) S300–S307.
[23] J. Sheng, H. Meng, R. Fox, A large eddy PIV method for turbulence dissipation rate estimation, Chem. Eng. Sci. 55 (2000) 4423–4434.
[24] K.R. Sreenivasan, On the universality of the Kolmogorov constant, Phys. Fluids 7 (1995) 2778–2784.
[25] E. Ståhl Wernersson, C. Trägårdh, Measurements and analysis of high-intensity turbulent characteristics in a turbine-agitated tank, Exp. Fluids 28 (2000) 532–545.
[26] J.V. Steinbuck, P.L.D. Roberts, C.D. Troy, A.R. Horner-Devine, F. Simonet, A.H. Uhlman, J.S. Jaffe, S.G. Monismith, P.J.S. Franks, An autonomous open-ocean stereoscopic PIV profiler, J. Atmos. Oceanic Technol. 27 (8) (2010) 1362–1380.
[27] T. Tanaka, J.K. Eaton, A correction method for measuring turbulence kinetic energy dissipation rate by PIV, Exp. Fluids 42 (2007) 893–902.
[28] H. Tennekes, J.L. Lumley, A First Course in Turbulence, The MIT Press, 1972.
[29] J. Westerweel, D. Dabiri, M. Gharib, The effect of a discrete window offset on the accuracy of cross-correlation analysis of digital PIV recordings, Exp. Fluids 23 (1997) 20–28.
[30] D. Xu, J. Chen, Experimental study of stratified jet by simultaneous measurements of velocity and density fields, Exp. Fluids 53 (2012) 145–162.